An enhanced nonlinear multi-scale strategy for the simulation of buckling and delamination on 3D composite plates

Karin Saavedra, Olivier Allix, Pierre Gosselet, J. Hinojosa, A. Viard

An enhanced nonlinear multi-scale strategy for the simulation of buckling and delamination on 3D composite plates

K. Saavedra[1], O. Allix[2], P. Gosselet[2], J. Hinojosa[1], A. Viard[2]
[1]Departamento de Tecnologías Industriales, Universidad de Talca. Chile.
[2]LMT Cachan (ENS Paris Saclay/CNRS/Université Paris Saclay). France.

March 24, 2021

Abstract

This paper is devoted to the study of a micro-macro LaTIn-based Domain Decomposition Method for which the partitioning, the geometry and the boundary conditions play a major role in the number of iterations to convergence and in the scalability. To confront these obstacles, an analysis of the macroscopic space and of the search direction – two parameters of the strategy – is proposed for traction, bending and buckling examples. Then, we propose a new search direction which takes into account the global stiffness of the structure and that limits the need to enrich the macroscopic space. This choice leads to a minimal number of iterations, a reduced computation time and the scalability of the strategy. The enhanced parameter is then applied to the simulation of combined buckling and delamination of a composite 3D plate.

Keywords: multi-scale simulation; domain decomposition; macroscopic basis; search direction; buckling; delamination

1 Introduction

Non overlapping Domain Decomposition Methods (DDMs) have been developed for the past two decades to solve partial differential equations on modern parallel computers. In particular, DDMs have emerged as powerful iterative algorithms to solve large systems arising from the finite element discretization of structure mechanics problems.

These parallel algorithms deal with local problems defined independently in each subdomain and with a global interface problem to enforce the continuity of the solution. In order to achieve better parallelism, the interface problem is typically solved with iterative algorithms. It is thus crucial to develop effective preconditioners and coarse problems to provide a mechanism for the global exchange of information on the whole structure and to maintain the convergence rate when increasing the number of subdomains (scalability).

Let us cite among the most widespread methods, the Finite Element Tearing and Interconnecting (FETI) [1], the Balancing Domain Decomposition (BDD) [2] – these methods differ in the interface unknowns: displacements (primal approach) or nodal reactions (dual approach) – and their constrained versions Dual-Primal FETI (FETI-DP) [3] and BDD with constraints (BDDC) [4]; a review of the most employed strategies can be found in [5]. Another technique is the so-called micro-macro LaTIn (LArge Time INcrement) approach [6] which can be considered as a two-scale DDM with Robin conditions on the interfaces (mixed approach). This method has been successfully applied to diverse nonlinear problems, e.g. contact problems [7], crack propagation [8, 9], delamination [10] and buckling-delamination interaction [11]. The enhanced nonlinear DDM proposed here is based on this multi-scale algorithm (more details in Sec. 2).

In order to obtain an efficient DDM, several obstacles must be overcome: a major issue is to optimize the load balancing of the processors and to reduce the interprocess communication. For this, DDMs require equal-size subdomains and minimal interface length. Moreover, additional constraints associated to the model or to the geometry must be taken into account in the partitioning of mechanical problems, like avoiding subdomains with bad aspect ratio [12], subdomains with irregular shapes [13], heterogeneities across the interfaces [14], inside the subdomains [15] or along the interfaces [16]. In those latter cases, DDMs need to deal with interface problems that are ill-conditioned and with a bad convergence rate. Recent contributions [17, 18, 19, 20] achieve robustness for linear problems through prior analysis and augmentation of the Krylov solver or multipreconditioning; in [21] a two scale approximation for the Robin parameter is proposed leading to a good convergence rate but at a high computational cost. However, classical DDMs are not yet robust technics in a nonlinear framework, specially when dealing with different interface behaviors or localized nonlinearities [22, 23, 24, 25].

From the DDMs' point of view, the LaTIn method is close to two-level optimized Schwarz methods [26], it is embedded in an alternating directions nonlinear solver [27]. This allows a huge flexibility and a simplified treatment of interface behaviors like contact, friction or cohesion. For instance, dealing with cohesive interfaces

between subdomains with FETI would not be so easy because, unlike perfect joint or contact, the interface relation is not a constraint to dualize. The price to pay for this flexibility is the use of a fixed point algorithm whose rate of convergence is slower than the one of Newton's approaches, not to mention the one of Krylov solvers in the linear case. Hence, the choice of the parameters of the method to ensure a reasonable rate of convergence is crucial. To the author's knowledge, there is no recent comparison, which would incorporate all recent improvements to the methods, between the LaTIn method and Newton-Schur approaches; the results of reference [6] are probably out of date.

In this work, we present a micro-macro LaTIn-based DDM in a large displacements context for the parallel simulation of composite laminates which are liable to delamination. In our approach, the composite plate is modeled on the mesoscale using plies separated by interfaces. All along these material interfaces, Cohesive Zone Models (CZM) [28] are implemented in order to compute potential delamination, then unilateral contact conditions are introduced by means of an interface law in order to avoid interpenetration when delamination occurs (see Fig. 2). In this work, the intralaminar degradations are neglected.

Firstly, this multi-scale strategy divides the structure into volume subdomains separated by (2D) interfaces, both of which are mechanical entities bearing kinematic and static unknowns as well as a constitutive equation. It is then natural to have the partitioning match the cohesive and contact zones, so that the material interfaces are handled at the interfaces of the domain decomposition.

Secondly, the strategy solves the partitioned problem using the micro-macro LaTIn algorithm. The LaTIn method is a computational algorithm for the resolution of time-dependent nonlinear problems that operate over the entire space-time domain [29, 30]. In our case, time is irrelevant and the capabilities of the LaTIn method are partially exploited. However, we use the idea of separating the difficulties and dealing with two sets of equations, the local stage and the admissibility stage, in order to reach the solution iteratively. These stages are linked by two interface "search directions" operators making the problem well-posed. The search directions are also interpreted as "interface impedances" (Robin conditions) [6], which are scalar parameters of the strategy representing the influence of neighboring subdomains and interfaces. Optimal and practical values have been determined for different mechanical problems as explained in Sect. 2.5.

The local stage solves problems on each Gauss point of the interfaces, while the admissibility stage defines problems with mixed (Robin) boundary conditions on every subdomains. These independent problems posed on interfaces and subdomains are the so-called **microscale** and correspond to the small-wavelength phenomena, which occur between neighboring subdomains. To ensure a good convergence rate and to achieve scalability, a global coarse problem weakly connects subdomains together in the admissibility stage. This coarse problem constitutes the **macroscale** and relates a few number of degrees of freedom per interface, which are defined by a macroscopic space and linked together by an homogenized behavior of the subdomains, in order to verify partially the equilibrium of the whole structure.

Although this coarse problem is similar to the one involved in other DDMs' second level projector, classically it has been called the "macroscopic problem" because it was inspired by the numerical homogenization of the subdomains and it is defined in a scale higher than the local problems posed on each subdomain and each interface. The macroscale aims at transferring the largest wavelength numerical information through the whole structure, in a way such that, according to the Saint-Venant principle, the complement, i.e. the microscale, only has a local influence. For this reason, the macroscopic space should contain the resultant forces and moments to transfer the global information while the micro complement should have zero resultant forces and moments to have localized effects.

The definition of an appropriate macroscopic space for the LaTIn method is a complex issue that has not yet been fully elucidated, because it depends on each type of problem, on its partition and even on the chosen Robin parameter [31], needing therefore additional calculations. Classically, when dealing with massive structures and interfaces with aspect ratio close to one, it has been shown that the macroscopic basis should extract the linear part of the interface quantities in order to ensure the scalability and that other additional terms do not have a major impact on the convergence rate [32, 8].

As shown in [11, 33], several numerical difficulties are encountered when applying the strategy to slender structures. For instance, the convergence rate and the scalability are degraded when using a linear macroscopic basis, so the search directions must be carefully adapted according to the geometry of the structure. However, these previous enhancements are not enough when dealing with more complex structures (e.g. 3D plates with slender subdomains and interfaces). Fig. 1 shows the influence of the geometry and of the partition on the number of iterations for a 3D bending problem of an uniformly loaded rectangular plate with built-in edges. In fact, a loss of efficiency is observed: the number of iterations increases when the plate's thickness decreases (see Fig. 1(a)) or when the number of subdomains increases (see Fig. 1(b)). Another issue is the dependency of the convergence rate on the type of load, i.e. the number of iterations is different for a bending or a traction problem, as shown in Sec. 3.1 and Sec. 3.2.

We aim at defining a micro-macro LaTIn-based DDM for which the convergence rate does not depend on the geometry, on the partitioning nor on the boundary conditions of the problem to solve. For this purpose, we

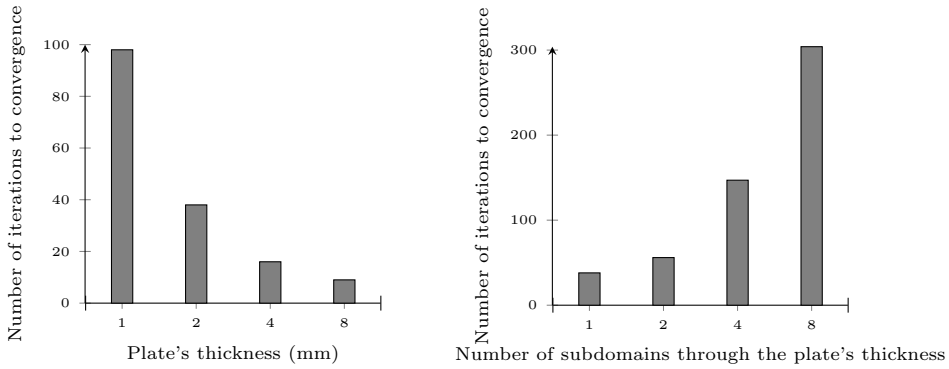

(a) Plate's geometry: $160 \times 120 \times x$ (mm). Partitioning: $16 \times 12 \times 1$ subdomains. Method's parameters: Linear macroscopic basis; $k^{-m}_{S_0S'_0} = E/L_{\Gamma_{S_0S'_0}}$; $(k^{-m}_{S_0S'_0})_n/(k^{-m}_{S_0S'_0})_t = 1$

(b) Plate's geometry: $160 \times 120 \times 2$ (mm). Partitioning: $16 \times 12 \times x$ subdomains. Method's parameters: Linear macroscopic basis; $k^{-m}_{S_0S'_0} = E/L_{\Gamma_{S_0S'_0}}$; $(k^{-m}_{S_0S'_0})_n/(k^{-m}_{S_0S'_0})_t = (L_0/h_0)^2$

Figure 1: Influence of a) the geometry and b) the partition on the convergence rate for a 3D bending plate.

study the influence of the two major parameters of the strategy – the macroscopic basis and the search directions – in 3D plate problems involving slender subdomains and interfaces. The objective is to find a macroscopic basis, a search direction or a combination of both that enables to reach convergence at the lowest numerical cost. Then, the optimal results from this analysis, for which we also found a physical interpretation, are used to achieve more efficient simulations of combined buckling and delamination of 3D composite plates.

This paper is organized as follows: Sec. 2 describes briefly the foundations of the micro-macro LaTIn-based DDM. The influence of the geometry, the partitioning and the boundary conditions on the convergence rate is highlighted in Sec. 3.1 and Sec. 3.2. Sec. 3.3 reviews the main results in order to reduce the number of iterations and to ensure the scalability of the method. From the proposed improvements, Sec. 4 exposes a buckling problem and a combined buckling and delamination simulation. Sec. 5 concludes the paper.

2 The multi-scale strategy

In this section, we briefly introduce the reference problem and the micro-macro LaTIn-based DDM, refer to [11] for a complete description of the method. The parameters under study are opportunely emphasized.

2.1 The reference problem and its partitioning

Let us consider a laminate composite (see Fig. 2) occupying the domain Ω bounded by $\partial\Omega$ in the current configuration, and consisting of N_P plies. Each ply P is connected to an adjacent ply P' through the interface $\Gamma_{PP'}$. The structure is subjected to an external surface traction field $\underline{F}_d$ on the part $\partial\Omega_{F_d}$ and to a displacement field $\underline{U}_d$ on the complementary part $\partial\Omega_{U_d}$. The body force per unit mass is written $\underline{f}_d$. The relevant quantities (*e.g.* volume, area or surface tractions) are described in reference to the undeformed configuration using the index $\cdot_0$.

We propose to study the mesoscopic response of the structure subjected to a prescribed dead loading (not a follower force) starting from the initial configuration, and resulting in large displacements and rotations

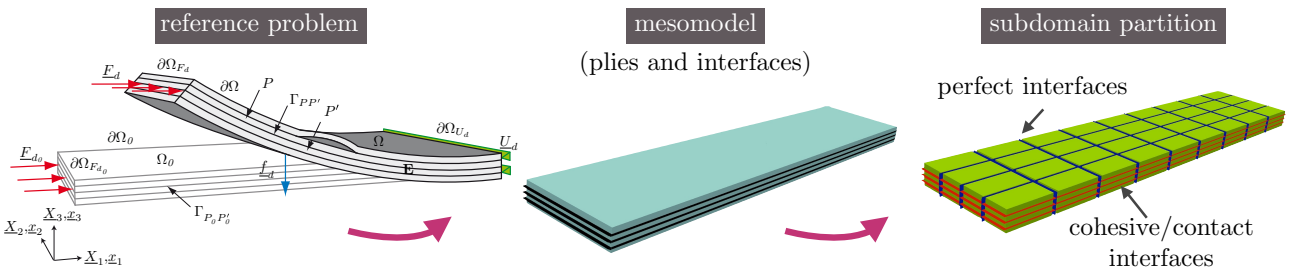

Figure 2: The reference problem, its mesomodel and its partitioning.

accompanied by progressive damage of the interfaces while the intralaminar degradations remain neglected. The geometrically nonlinear evolution is handled through a total Lagrangian formulation and delamination is modeled using a Cohesive Zone Model (CZM). In delaminated regions, the interface behavior becomes unilateral contact.

A CZM can be described as a zero thickness interface where tractions (i.e. the normal Cauchy stresses $\underline{t} = \underline{\underline{\sigma}} \cdot \underline{n}$, $\underline{n}$ being the vector normal to the interface) are related to the displacement jump of the interface $[\underline{u}]$ by the mean of a softening function. This evolution law can be written in terms of a damage variable d, like $\underline{t} = (1-d)\underline{\underline{k}}_0[\underline{u}]$ with d ranging from 0 (healthy interface point) to 1 (completely damaged interface point) and $\underline{\underline{k}}_0$ the initial interface stiffness with no damage.

When the structure is loaded, the cohesive interface opens while transferring normal stresses from one face to the other. The stiffness decreases with respect to the displacement jump and becomes zero for some critical displacement jump. In this work, we adopt the CZM proposed in [34], which is based on damage mechanics. We refer to [34, 35] for an extensive description of the model.

Regarding the partitioning, as presented in Fig. 2, the structure is split into subdomains which are connected by interfaces. The partitioning process makes the domain decomposition interfaces match with the material interfaces (cohesive or contact), so that each subdomain belongs to a unique ply. A subdomain S_0 defined in the undeformed domain Ω_{S_0} is connected to an adjacent undeformed subdomain S_0' through an undeformed interface $\Gamma_{S_0S_0'} = \partial\Omega_{S_0} \cap \partial\Omega_{S_0'}$. The surface entity $\Gamma_{S_0S_0'}$ applies force distributions $(\underline{F}_{S_0S_0'}, \underline{F}_{S_0'S_0})$ and displacement distributions $(\underline{W}_{S_0S_0'}, \underline{W}_{S_0'S_0})$ to S_0 and S_0', respectively.

The purpose of the method is to find the subdomain fields $\underline{u}_{S_0}$ (displacement) and $\underline{\underline{\pi}}_{S_0}$ (second Piola-Kirchhoff stress), and the interface fields $\underline{W}_{S_0}$ (displacement) and $\underline{F}_{S_0}$ (inter-forces), where the index S ranges over all subdomains. These kinematic and static unknowns are related by constitute laws, which define local problems in the subdomains and in the interfaces, respectively.

2.2 Governing equations

The governing equations of the system are split into two groups:

- local equations in the interfaces whose solutions form the manifold $\mathbf{L}_\Gamma$:
  - constitutive relation of the interfaces (perfect, contact and cohesive interfaces) and boundary conditions, which can be formally written as:
$$\mathcal{R}_{S_0S_0'}([\underline{W}]_{S_0S_0'}, \underline{F}_{S_0S_0'}, \underline{F}_{S_0'S_0}) = \underline{0} \tag{1}$$
    where $[\underline{W}]_{S_0S_0'} = \underline{W}_{S_0S_0'} - \underline{W}_{S_0'S_0}$ is the displacement gap at the interface.
  - static admissibility of the interfaces: for all considered behaviors, interface tractions satisfy the following action-reaction principle:
$$\underline{F}_{S_0S_0'} + \underline{F}_{S_0'S_0} = \underline{0} \tag{2}$$
- equations in the subdomains and macroscopic admissibility of interfaces, whose solutions form the manifold $\mathbf{A_d}$:
  - nonlinear kinematic admissibility of the subdomains
$$\underline{\underline{E}}_{S_0} = \frac{1}{2}\left(\nabla\underline{u}_{S_0} + {}^t\nabla\underline{u}_{S_0} + {}^t\nabla\underline{u}_{S_0} \cdot \nabla\underline{u}_{S_0}\right) \text{ , on } \Omega_{S_0} \tag{3}$$
$$\underline{u}_{S_0|\Gamma_{S_0S_0'}} = \underline{W}_{S_0S_0'} \tag{4}$$
  - nonlinear static admissibility of the subdomains
$$\forall \underline{u}^\star_{S_0} \in \mathcal{U}^0_{S_0},$$
$$\int_{\Omega_{S_0}} \underline{\underline{\pi}}_{S_0} : \underline{\underline{E}}^\star(\underline{u}^\star_{S_0})\, d\Omega_0 = \int_{\Omega_{S_0}} \rho_{S_0}\, \underline{f}_d \cdot \underline{u}^\star_{S_0}\, d\Omega_0 + \sum_{S_0'} \int_{\Gamma_{S_0S_0'}} \underline{F}_{S_0S_0'} \cdot \underline{u}^\star_{S_0}\, d\Gamma_0 \tag{5}$$
    where $\mathcal{U}^0_{S_0}$ is the subdomain displacements space with zero Dirichlet boundary conditions and $\underline{\underline{E}}^\star(\underline{u}^\star_{S_0}) = \frac{1}{2}(\nabla\underline{u}^\star_{S_0} + {}^t\nabla\underline{u}^\star_{S_0} + {}^t\nabla\underline{u}_{S_0} \cdot \nabla\underline{u}^\star_{S_0} + {}^t\nabla\underline{u}^\star_{S_0} \cdot \nabla\underline{u}_{S_0})$.

- hyperelastic orthotropic constitutive relation of the subdomains

$$\underline{\underline{\pi}}_{S_0} = \frac{\partial \psi}{\partial \underline{\underline{E}}_{S_0}} \text{ , over } \Omega_{S_0} \tag{6}$$

where ψ is the stored energy function or elastic potential per unit of undeformed volume. We use $\psi = \frac{1}{2}\underline{\underline{E}}_{S_0} : \mathbf{K}_{S_0} : \underline{\underline{E}}_{S_0}$.

- macroscopic admissibility of the interfaces (after the linearization of the previous equations), which is a partial verification of the action-reaction principle (2):

$$\forall \underline{W}^M \in \mathcal{W}^M_{S_0S'_0}, \quad \int_{\Gamma_{S_0S'_0}} (\underline{F}_{S_0S'_0} + \underline{F}_{S'_0S_0}) \cdot \underline{W}^M \, d\Gamma_0 = 0 \tag{7}$$

where the subspace $\mathcal{W}^M_{S_0S'_0}$ of interface macroscopic admissible displacements is a parameter of method described in Sec. 2.4.

2.3 The LaTIn iterative algorithm

The interface solution s_{ref} is such that $s_{ref} \in \mathbf{A_d} \cap \mathbf{L}_\Gamma$. A stationary algorithm is chosen where the solution s_{ref} is alternatively sought in these two manifolds: first, one finds a solution $s = (\underline{W}_{S_0S'_0}, \underline{F}_{S_0S'_0})$ in $\mathbf{A_d}$, then a solution $\hat{s} = (\hat{\underline{W}}_{S_0S'_0}, \hat{\underline{F}}_{S_0S'_0})$ in $\mathbf{L}_\Gamma$. In order for the two steps to be well-posed, one introduces the search directions k^+ and k^-, two parameters of the method, which link the solutions s and $\hat{s}$ during the iterative process. Thus, an iteration of the algorithm consists of two steps: the local stage ($\mathbf{L}_\Gamma$) and the admissibility stage ($\mathbf{A_d}$). For the sake of simplicity, a brief exposition of this iterative process is given in this article while a complete description can be found in [11].

Remark: The subscript $\cdot_{S_0S'_0}$ refers to variables defined in the interface $\Gamma_{S_0S'_0}$ while the subscript $\cdot_{S_0}$ is for quantities defined on the subdomain S_0. The circumflex accent $\hat{\cdot}$ is used to note the interface unknowns of the local stage and the superscript $\cdot^M$ refers to the macroscopic quantities.

The local stage: In this stage, the following local problem is solved at each Gauss point of the interfaces $\Gamma_{S_0S'_0}$:

Find $(\hat{\underline{F}}_{S_0S'_0}, \hat{\underline{W}}_{S_0S'_0}, \hat{\underline{F}}_{S'_0S_0}, \hat{\underline{W}}_{S'_0S_0})$ such that:

$$\mathcal{R}_{S_0S'_0}([\hat{\underline{W}}]_{S_0S'_0}, \hat{\underline{F}}_{S_0S'_0}, \hat{\underline{F}}_{S'_0S_0}) = \underline{0} \tag{8}$$

$$\hat{\underline{F}}_{S_0S'_0} + \hat{\underline{F}}_{S'_0S_0} = \underline{0} \tag{9}$$

$$(\hat{\underline{F}}_{S_0S'_0} - \underline{F}_{S_0S'_0}) - k^+_{S_0S'_0}(\hat{\underline{W}}_{S_0S'_0} - \underline{W}_{S_0S'_0}) = \underline{0} \tag{10}$$

$$(\hat{\underline{F}}_{S'_0S_0} - \underline{F}_{S'_0S_0}) - k^+_{S'_0S_0}(\hat{\underline{W}}_{S'_0S_0} - \underline{W}_{S'_0S_0}) = \underline{0} \tag{11}$$

The last two equations of this system define the search direction k^+ which couples the interface displacements and the interface forces. The setting of this parameter is discussed in the Sec. 2.5.

The admissibility stage: In this stage, we solve the system of nonlinear equations in the subdomains (3 - 6) together with the macroscopic admissibility constraint (7), using a finite element discretization and an iterative Newton-Raphson procedure (superscript i).

$\forall \underline{u}^\star_{S_0} \in \mathcal{U}^0_{S_0}$,

$$\int_{\Omega_{S_0}} \mathbf{K}_{S_0} \underline{\underline{E}}_{S_0}({}^i\underline{u}_{S_0}) : \left({}^t\nabla {}^i\delta\underline{u}_{S_0} \cdot \nabla \underline{u}^\star_{S_0} + {}^t\nabla \underline{u}^\star_{S_0} \cdot \nabla {}^i\delta\underline{u}_{S_0} \right) d\Omega_0 + \int_{\Omega_{S_0}} \mathbf{K}_{S_0} \underline{\underline{E}}^\star({}^i\delta\underline{u}_{S_0}) : \underline{\underline{E}}^\star(\underline{u}^\star_{S_0}) \, d\Omega_0 = {}^i\tilde{P}_{ext} + P_{int}({}^i\underline{u}_{S_0}) \tag{12}$$

where:

$${}^i\tilde{P}_{ext} = \int_{\Omega_{S_0}} \rho_{S_0} \underline{f}_d \cdot \underline{u}^\star_{S_0} \, d\Omega + \sum_{S'_0} \int_{\Gamma_{S_0S'_0}} {}^i\underline{F}_{S_0S'_0} \cdot \underline{u}^\star_{S_0} \, d\Gamma_0$$

$$P_{int}({}^i\underline{u}_{S_0}) = \int_{\Omega_{S_0}} \mathbf{K}_{S_0} \underline{\underline{E}}_{S_0}({}^i\underline{u}_{S_0}) : \underline{\underline{E}}^\star(\underline{u}^\star_{S_0}) \, d\Omega_0$$

$${}^{i+1}\underline{u}_{S_0} = {}^i\underline{u}_{S_0} + {}^i\delta\underline{u}_{S_0}$$

$$\underline{\underline{E}}^\star({}^i\delta\underline{u}_{S_0}) = \frac{1}{2}(\nabla {}^i\delta\underline{u}_{S_0} + {}^t\nabla {}^i\delta\underline{u}_{S_0} + {}^t\nabla \underline{u}_{S_0} \cdot \nabla {}^i\delta\underline{u}_{S_0} + {}^t\nabla {}^i\delta\underline{u}_{S_0} \cdot \nabla \underline{u}_{S_0})$$

The system is closed by a search direction which takes the following form:

$$\forall \underline{W} \in \mathcal{W}_{S_0S_0'}, \quad \int_{\Gamma_{S_0S_0'}} ({}^i\underline{F}_{S_0S_0'} - \hat{\underline{F}}_{S_0S_0'}) \cdot \underline{W}\, d\Gamma_0 + \int_{\Gamma_{S_0S_0'}} \left(k^-_{S_0S_0'} ({}^i\underline{W}_{S_0S_0'} - \hat{\underline{W}}_{S_0S_0'}) - k^-_{S_0S_0'} {}^i\widetilde{\underline{W}}^M_{S_0S_0'} \right) \cdot \underline{W}\, d\Gamma_0 = 0 \quad (13)$$

were $\mathcal{W}_{S_0S_0'}$ is the kinematically admissible interface displacements space, $k^-_{S_0S_0'}$ is the operator which characterizes the search direction and ${}^i\widetilde{\underline{W}}^M_{S_0S_0'} \in \mathcal{W}^M_{S_0S_0'}$ is the unknown Lagrangian multiplier (homogeneous to a displacement) necessary to satisfy the macroscopic constraint (7).

In the end, the admissibility stage takes the form of Robin problems set on subdomains linked by the macroscopic constraint. It is possible to isolate the unknown $({}^i\widetilde{\underline{W}}^M_{S_0S_0'})$ by static condensation, assemble what we call the "macroscopic problem", solve it (with a direct or an iterative solver [10]) and then obtain the subdomains' displacement $({}^{i+1}\underline{u}_{S_0})$ by independent computations.

Convergence of the algorithm: In order to evaluate the convergence of the iterative process, a criterion based on the verification of the constitutive laws of the interfaces quantities issued from the admissibility stage has been implemented. A complete description of this error indicator can be found in [36].

2.4 The macroscopic space

In order to ensure the scalability of the iterative scheme, the global linear coarse grid problem (7) has been introduced. It is fully characterized by the set of interface macroscopic spaces $(\mathcal{W}^M_{S_0S_0'})$ which are defined by a macroscopic basis $\mathcal{B}^M_{S_0S_0'} = \left(\underline{e}^M_1, \ldots, \underline{e}^M_{N_M}\right)$ for each interface $\Gamma_{S_0S_0'}$.

Classically, it has been accepted that the macroscopic space should contain at least the affine part of the interface displacements in order to ensure scalability; this corresponds to ensuring the balance of the first moments of forces at the interface using the first six basis vectors illustrated in Fig. 3. However, as shown in Fig. 1, if slender structures are involved, the generally accepted linear macroscopic basis which considers nine basis vectors (see Fig. 3) is not enough to ensure a good convergence rate. To palliate this problem, we propose to enrich the macroscopic space including quadratic and cubic functions in the macroscopic basis, as shown in Fig. 3. A presents the construction of the complete basis $\mathcal{B}^M_{E_0E_0'}$ for the macroscopic space of a plane interface.

Remark: The subspace of microscopic displacement $\mathcal{W}^m_{S_0S_0'}$ which is supplementary to $\mathcal{W}^M_{S_0S_0'}$ in $\mathcal{W}_{S_0S_0'}$ is orthogonal (in the sense of the interface mechanical work) to the subspace of macroscopic traction which is defined by $\mathcal{F}^M_{S_0S_0'} = k^-_{S_0S_0'}\mathcal{W}^M_{S_0S_0'}$; the subspace of microscopic interface tractions is defined likewise. These definitions enable us to decompose (in a unique way) any interface force or displacement into a macroscopic and a microscopic contribution.

2.5 The search directions

The search direction parameters are operators which represent the influence of the neighboring subdomains and interfaces. The optimal value is the Schur complement of the rest of the structure. In general, a very coarse approximation, in practice a scalar, is sufficient to ensure a good convergence rate of the LaTIn method. It has been empirically shown that an optimal set of search directions exists, depending on the interface behavior, but these operators are known to be difficult to interpret theoretically, as exposed in [37, 6, 11].

In order to find the most favorable values, it is convenient to choose $k^-_{S_0S_0'}$ to be block diagonal in the micro/macro decomposition of interface subspaces. We thus define the macroscopic and the microscopic part (respectively $k^{-M}_{S_0S_0'}$ and $k^{-m}_{S_0S_0'}$) of the search direction. For this reason, Eq. (13) can be rewritten as:

$$\forall\, \underline{W}^M \in \mathcal{W}^M_{S_0S_0'}, \quad \int_{\Gamma_{S_0S_0'}} ({}^i\underline{F}_{S_0S_0'} - \hat{\underline{F}}_{S_0S_0'}) \cdot \underline{W}^M\, d\Gamma_0 + \int_{\Gamma_{S_0S_0'}} k^{-M}_{S_0S_0'} ({}^i\underline{W}_{S_0S_0'} - \hat{\underline{W}}_{S_0S_0'} - {}^i\widetilde{\underline{W}}^M_{S_0S_0'}) \cdot \underline{W}^M\, d\Gamma_0 = 0 \quad (14)$$

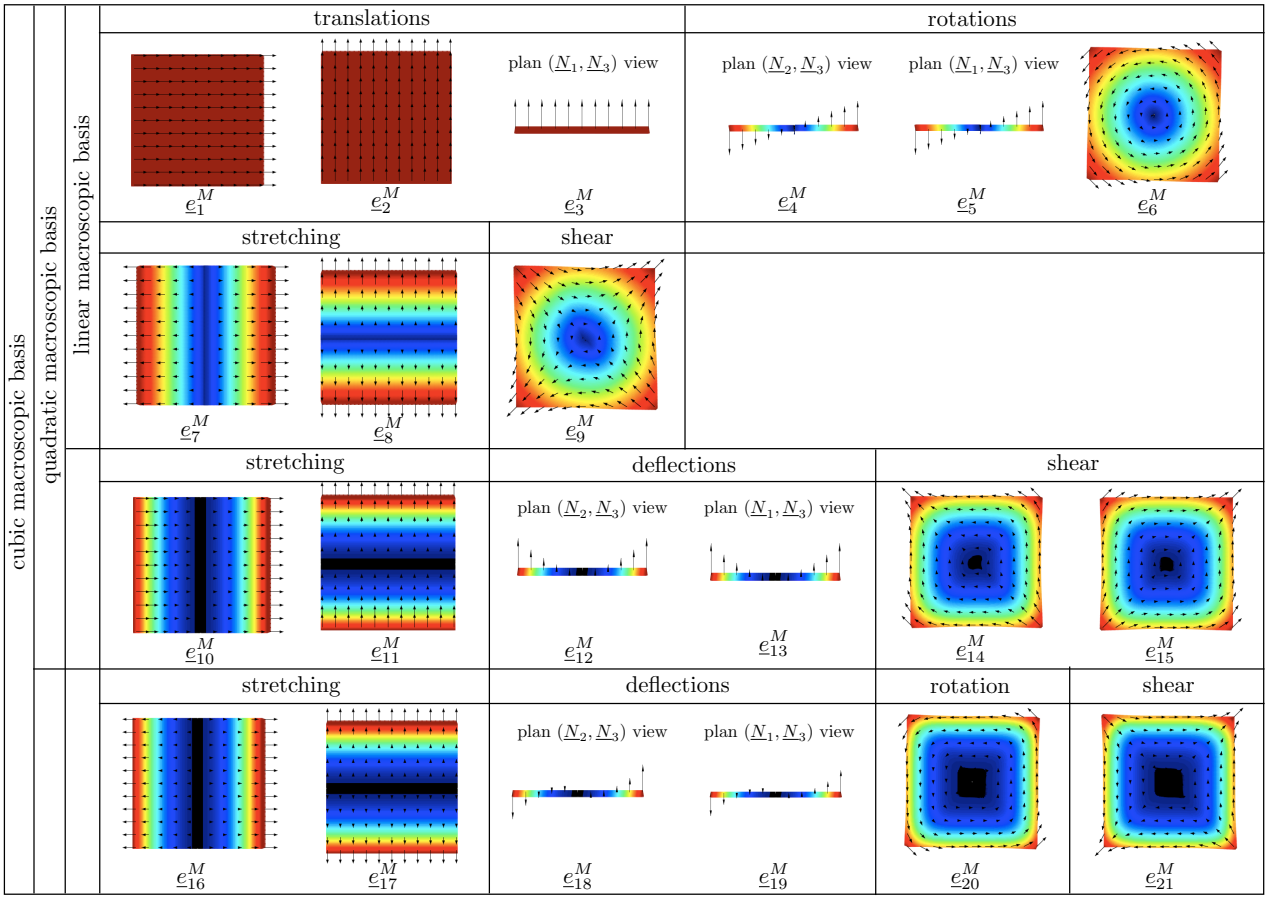

Figure 3: The macroscopic bases for a plane interface (linear, quadratic and cubic).

$$\forall\ \underline{W}^m \in \mathcal{W}^m_{S_0S'_0},\quad \int_{\Gamma_{S_0S'_0}} ({}^i\underline{F}_{S_0S'_0} - \hat{\underline{F}}_{S_0S'_0}) \cdot \underline{W}^m \, d\Gamma_0 + \int_{\Gamma_{S_0S'_0}} k^{-m}_{S_0S'_0} \, ({}^i\underline{W}_{S_0S'_0} - \hat{\underline{W}}_{S_0S'_0}) \cdot \underline{W}^m \, d\Gamma_0 = 0 \quad (15)$$

Parameter $k^{-M}_{S_0S'_0}$ represents the stiffness of the interface for the macroscopic problem.

For perfect interfaces (i.e. infinite stiffness), $k^{-M}_{S_0S'_0}$ must be as large as possible. Parameter $k^{-m}_{S_0S'_0}$ is the microscopic part of the search direction and it has been widely accepted that it has a localized effect. In practice, the classical setting for homogeneous structures with perfect interfaces is $k^{-m}_{S_0S'_0} = E/L_{\Gamma_{S_0S'_0}}$, where E is Young's modulus and $L_{\Gamma_{S_0S'_0}}$ is a characteristic length of the interface [6]. The local search direction $k^{+}_{S_0S'_0}$ is usually set equals to the microscopic search direction $k^{-m}_{S_0S'_0}$. Besides, it was shown that for 3D beams in bending, the slenderness induces a structural anisotropy that can be taken into account by the search directions [11]. A dimensional analysis leads to the following relationship between the longitudinal (n) and transverse (t) search directions (L_0 is the characteristic length of the structure, h_0 is its thickness):

$$\frac{\left(k^{-m}_{S_0S'_0}\right)_n}{\left(k^{-m}_{S_0S'_0}\right)_t} = \left(\frac{L_0}{h_0}\right)^2 \quad (16)$$

This modification leads to a better convergence rate and ensures the scalability for slender 3D beams, without adding supplementary terms to the linear macroscopic basis. With this adaptation, $k^{-m}_{S_0S'_0}$ contains information about the stiffness of the structure, which spares us from enriching the macroscopic basis in order to transfer the large wavelength information. Thus, the anisotropic relation becomes a easy alternative to reduce the computing time, but this implies to input a global information at the interface scale, which is not classical.

In the case of cohesive interfaces, when solving the nonlinear system of Eqs. (8-11) with a Newton-Raphson method some solutions in the softening part of the local cohesive behavior are unreachable, as explained in [10]. To avoid the stagnation or the divergence of the strategy, the local search directions $k^{+}_{S_0S'_0}$ must be formally set

to infinite values. In practice, this choice leads to calculate directly the interface's quantities in the local stage: Eqs. (10) and (11) become $\underline{\hat{W}}_{S_0S_0'} = \underline{W}_{S_0S_0'}$ and $\underline{\hat{W}}_{S_0'S_0} = \underline{W}_{S_0'S_0}$, and local Newton's iterations are unnecessary to calculate $(\underline{\hat{F}}_{S_0S_0'}, \underline{\hat{F}}_{S_0'S_0})$. Concerning search direction $k^-_{S_0S_0'}$, the optimal value would be twice the actual interface stiffness, $k^{-m}_{S_0S_0'} = k^{-M}_{S_0S_0'} = 2k^0(1-d)$ (k^0 denoting the undamaged interface's local stiffness), which would be equivalent to prescribing the exact interface behavior as an interface condition in the admissibility stage [10]. Unfortunately, the use of this value would require the operators to be updated very frequently, which would be expensive; instead, a monitoring strategy has been proposed in [10, 11].

In the case of contact interfaces for slender structures, the use of search directions $k^+_{S_0S_0'} = k^{-m}_{S_0S_0'} = k^{-M}_{S_0S_0'} = E/L_{\Gamma_{S_0S_0'}}$ for the closed interfaces and $k^+_{S_0S_0'} = k^{-m}_{S_0S_0'} = k^{-M}_{S_0S_0'} = 0$ for the separated interfaces results in a proper macroscopic problem (representing the stiffness of the contact interface) and a correct converged solution, as explained in [11]. However, in practice, a unified value equal to $k^+_{S_0S_0'} = k^-_{S_0S_0'} = (E/L_{\Gamma_{S_0S_0'}})/(L_0/h_0)^2$ is used to avoid updating the state of the interface (i.e. open or close).

The value $E/L_{\Gamma_{S_0S_0'}}$ for the search direction of perfect interfaces has been previously related to traction problems [6], therefore we propose to investigate its pertinence to bending and buckling problems.

3 Analysis of the parameters

The aim of this section is to understand the influence of the two major parameters of the method – the search directions and the macroscopic basis – for the analysis of 3D slender plates. To begin with, geometric nonlinearities and delamination are omitted, i.e. linear calculations in one load increment are performed and only perfect interfaces are considered. We observe the convergence rate of the strategy for the simulation of a 3D plate lying in the X_1X_2-plane under two loading conditions:

- **Bending** of a orthotropic rectangular plate built-in along its four edges. An uniform load $q = 0.1$ [N/mm^2] is distributed over the upper surface in direction $-X_3$;
- **Traction** of a orthotropic rectangular plate with two opposite sides free; the third edge is built-in and the fourth edge is subjected to a uniform traction displacement $U = 1$ [mm] in direction X_1.

The plate is made out of a 0° layer of carbon fibre reinforced plastic IM7/8552 whose homogenised elastic constants are: E_1=165,000 [MPa], E_2=E_3=9000 [MPa], G_{12}=G_{13}= 5600 [MPa], G_{23}=2800 [MPa], ν_{12}=ν_{13}=0.34 and ν_{23}=0.5 [38]. The dimensions on the X_1X_2 plane are fixed to $L_{X_1} = 160$ [mm] and $L_{X_2} = 120$ [mm] while different thicknesses are studied - $h = 1$ [mm], $h = 2$ [mm], $h = 4$ [mm] and $h = 8$ [mm] - keeping constant the number of subdomains to 192 (see Sec. 3.1). Furthermore, for a given geometry ($L_{X_1} = 160$ [mm], $L_{X_2} = 120$ [mm] and $h = 2$ [mm]), three partitions – 192, 384 and 768 subdomains – are analyzed in Sec. 3.2. It is important to note that the studied configurations are chosen because we are interested in the simulation of laminate composite made of multiple slender layers.

Both load cases are analyzed under the following possibilities:

- using a linear, quadratic or cubic **macroscopic basis** (as defined in Sec. 2.4);
- multiplying the classic value of the **search direction** $k^+_{S_0S_0'} = k^{-m}_{S_0S_0'} = E/L_{\Gamma_{S_0S_0'}}$ by a search direction factor $\alpha \in [10^{-6}, 100]$, while the parameter $k^{-M}_{S_0S_0'}$ is fixed to an extremely large value.
- considering the **anisotropic relation** of the search direction or not. For this, the characteristic length of the structure has been calculated as $L_0 = 0.5(L_{X_1} + L_{X_2})$.

The plate is modeled using a finite element mesh with 264,960, 529,920 or 1,059,840 linear wedge elements (with 10 elements through-the-thickness of the subdomain) and near to 500 thousand, 1 million or 2 million DOFs, depending on the partitioning (192, 384 and 768 subdomains, respectively). This difference is due to the fact that the number of DOFs per subdomain is the same for all the partitions. All the computations were carried out using a fully parallel finite element program, implemented in a C++ research code, where the transfers of data were performed using MPI libraries. Because subdomains are relatively small, a set of connected subdomains (with their interfaces) is assigned to each MPI process; this assignment is achieved using a METIS routine. 64 processors are used for the parallel simulations.

3.1 Influence of the geometry

In this section, the number of iterations for different thicknesses ($h = 1$ [mm], $h = 2$ [mm], $h = 4$ [mm] and $h = 8$ [mm]) is analyzed. The dimensions $L_{X_1} = 160$ [mm] and $L_{X_2} = 120$ [mm] are constant and the partitioning

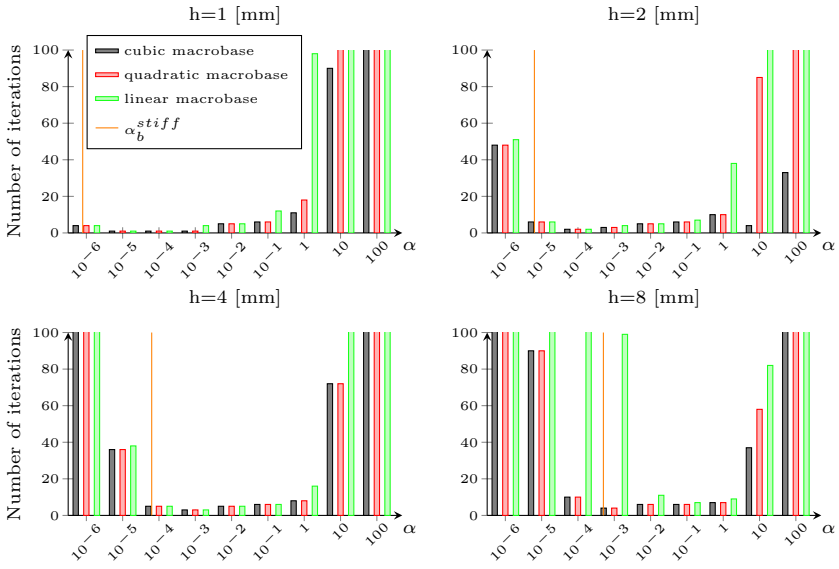

Figure 4: Iterations to convergence vs. search direction factor for different plate's thickness. $16 \times 12 \times 1$ subdomains. Bending load. $(k^{-m}_{S_0S'_0})_n/(k^{-m}_{S_0S'_0})_t = 1$.

is fixed to 16 subdomains in direction X_1, 12 subdomains in direction X_2 and one subdomain through-the-thickness. For the sake of clarity in the presentation of the results, the number of iterations is truncated to 100 in the plots.

Bending: Fig. 4 shows the iterations of the bending problem for the three macroscopic bases (linear, quadratic and cubic) and for the search direction factor α which is comprised in the set of values $[10^{-6}, 100]$. In these calculations, the anisotropic relation of the search directions has not been taken into account ($(k^{-m}_{S_0S'_0})_n/(k^{-m}_{S_0S'_0})_t = 1$). From Fig. 4, we can observe that for each thickness, there is an optimal value of the search direction factor for which the iterations are minimal and equal for the three macroscopic bases (except for the case of $h = 8$ [mm] for which it is valid only for the quadratic and cubic bases), that is $\alpha^{opt_b}_{h=1} \in [10^{-5}, 10^{-4}]$ (1 iteration), $\alpha^{opt_b}_{h=2} = 10^{-4}$ (2 iterations), $\alpha^{opt_b}_{h=4} = 10^{-3}$ (3 iterations) and $\alpha^{opt_b}_{h=8} = 10^{-3}$ (2 iterations). When the classical search direction (i.e. $\alpha = 1$) and the linear macroscopic basis are adopted, the number of iterations increases when the plate thickness decreases, reaching near to one hundred iterations for $h = 1$ [mm].

If the anisotropic relation of the search directions is used, the optimal search direction factor α^{opt_b} remains unchanged for all the geometries, the minimal number of iterations is similar (1, 1, 2 and 3 iterations respectively for $h = 1$, $h = 2$, $h = 4$ and $h = 8$ [mm]) and the variation between the three macroscopic bases is less significant than when using $(k^{-m}_{S_0S'_0})_n/(k^{-m}_{S_0S'_0})_t = 1$, as shown in Fig. 5. Moreover, the number of iterations is almost constant (between 6 and 10 iterations) for the three bases and for the four geometries when using the classical search direction (i.e. $\alpha = 1$). It is important to note that, in general, the number of iterations decreases when adopting the anisotropic relation of the search directions or when using the cubic macroscopic basis, nevertheless, the number of iterations is minimal and almost the same if the optimal value of the search direction factor is used, independently of the macroscopic basis (except for $h = 8$ [mm]), the geometry or the anisotropic relation.

In Fig. 4 and Fig. 5, the search direction factor α_b^{stiff} for which the search direction ($k^{+}_{S_0S'_0} = k^{-m}_{S_0S'_0}$) is equal to the global stiffness of the structure (the ratio of the applied load and the maximum deflection) has been identified. This value is remarkably close to the optimal search direction factor for the four geometries, there is a difference of a factor of 10 for each geometry (except for the case $h = 8$ for which both factors are equals), and gives a number of iteration close to the minimal (between 4 and 7 iterations).

Traction: The number of iterations of the traction problem is shown in Fig. 6 for the three macroscopic bases and the different search direction factors, without taking into account the anisotropic relation of the search directions. For this load case, the difference between the macroscopic bases is less relevant than in the bending problem, being more constant the number of iterations for the three bases. The minimal number of iterations (between 1 and 2 iterations) is reached when $\alpha^{opt_t} = 10^{-1}$ for the four thicknesses. The classical search direction (i.e. $\alpha = 1$) takes one more iteration than the optimal choice to attain the same precision. Adopting the anisotropic relation, the same behavior as in Fig. 6 has been found, without a significant variation in the number of iterations. Because this resemblance, those results were omitted for the sake of simplicity. This fact is natural because the tangential and normal separation of the anisotropic relation is only activated in bending; in traction only normal stresses are involved.

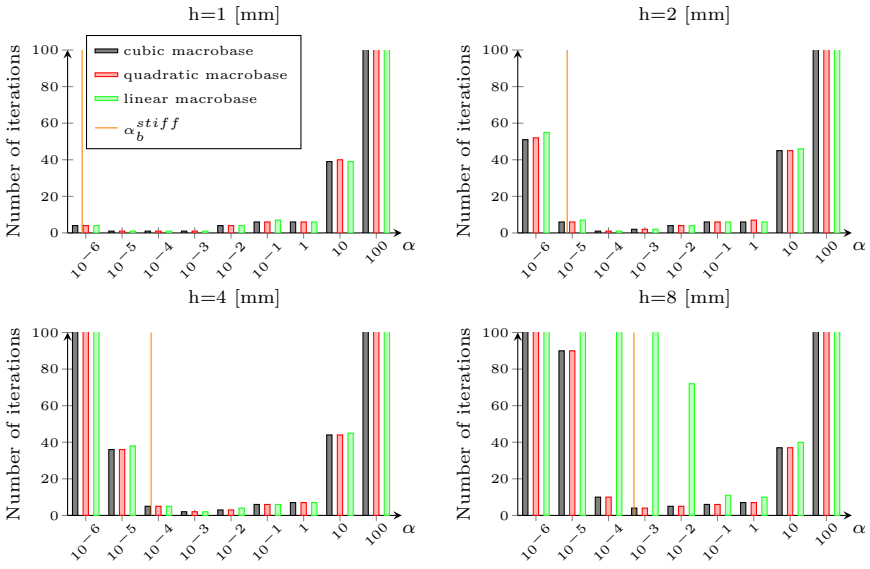

Figure 5: Iterations to convergence vs. search direction factor for different plate's thickness. $16 \times 12 \times 1$ subdomains. Bending load. $(k^{-m}_{S_0S'_0})_n/(k^{-m}_{S_0S'_0})_t = (L_0/h_0)^2$.

The search direction factor α_t^{stiff} for which the search direction ($k^{+}_{S_0S'_0} = k^{-m}_{S_0S'_0}$) is equal to the global stiffness of the structure (ratio of the applied load and the axial displacement) is shown in Fig. 6. This value coincides with the optimal search direction factor for the four geometries.

3.2 Influence of the partitioning

The number of iterations for different partitions but the same geometry ($L_{X_1} = 160$ [mm], $L_{X_2} = 120$ [mm] and $h = 2$ [mm]) is analyzed in this section. We consider 1, 2 or 4 subdomains through-the-thickness, while the directions X_1 and X_2 are always divided in 16 and 12 subdomains, respectively. The number of iterations is studied for the three macroscopic bases and for the search direction factor α included in the set of values $[10^{-6}, 1]$. As for previous section, the number of iterations is truncated to 100.

Bending: The influence of the partitioning for the bending problem without taking into account the anisotropic relation of the search direction is presented in Fig. 7 and considering the anisotropic relation in Fig. 8. For both cases, if the classical search direction, $\alpha = 1$, is adopted, the number of iterations increases when more subdomains are considered, reaching over one hundred iterations, i.e. a loss of scalability is observed. Generally, using the linear macroscopic basis, the number of iterations is higher than using the others macroscopic bases. However, there is an optimal search direction factor, $\alpha_{h=2}^{opt_b} = 10^{-4}$, for which the number of iterations is equal to 1 (except for the case with $16 \times 12 \times 1$ subdomains and $(k^{-m}_{S_0S'_0})_n/(k^{-m}_{S_0S'_0})_t = 1$ for which 2 iterations are needed) for the three macroscopic bases, considering or not the anisotropic relation, and for the three partitions (i.e. the scalability is recovered). As the precedent analysis in bending, the search direction factor α_b^{stiff} for which the search direction is equal to the global stiffness of the structure is very close to the optimal search direction factor for the three partitions (10 times suppler), attaining a similar number of iterations (between 1 and 6 iterations) and ensuring scalability.

Traction: Fig. 9 shows the number of iterations for the traction problem without the anisotropic relation ($(k^{-m}_{S_0S'_0})_n/(k^{-m}_{S_0S'_0})_t = 1$). In this case, the number of iterations are similar for the different partitions and they are not influenced by the macroscopic basis. It is possible to achieve the solution in 1 iteration when the search direction factor is in the range $\alpha_{h=2}^{opt_t} \in [10^{-2}, 10^{-1}]$. If the classical search direction (i.e. $\alpha = 1$) is adopted, convergence is reached in 1 or 2 iterations. The global stiffness of the structure (represented by α_t^{stiff}) agrees with the optimal search direction for the three partitions. Same conclusions have been found using the anisotropic relation of the search direction.

3.3 Discussion of the results

The major conclusions issued from the study carried out in Sec. 3 are summarized as follows:

- The convergence rate is highly dependent not only on the parameters of the method – the search direction and the macroscopic basis – but also on the load case, the geometry of the structure and the partitioning.

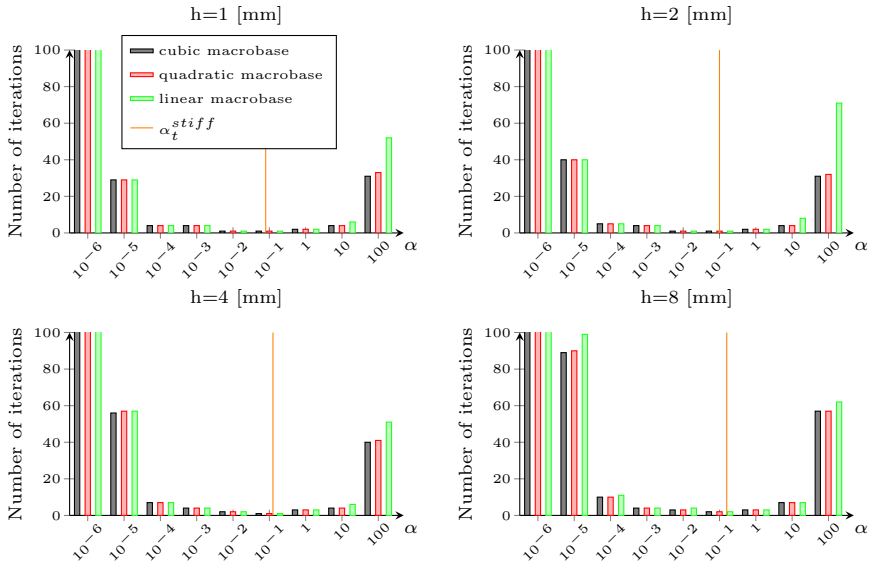

Figure 6: Iterations to convergence vs. search direction factor for different plate's thickness. $16 \times 12 \times 1$ subdomains. Traction load. $(k^{-m}_{S_0S_0'})_n/(k^{-m}_{S_0S_0'})_t = 1$.

- For each analyzed geometry and load case, there is an optimal search direction factor for which the number of iterations is minimal and the scalability is ensured. This optimal value is constant for the different partitions and for the three macroscopic bases (except $h = 8$ [mm] for which it is valid only for the quadratic and cubic bases).
- In general, when using the quadratic and cubic macroscopic bases, the number of iterations is smaller than when employing the linear macroscopic basis. Besides, quadratic and cubic macroscopic bases have similar results, except for some large search direction factors for which the cubic macroscopic basis is better. However, when the optimal search direction is adopted, the linear macroscopic basis is the most reasonable alternative (except for the case of $h = 8$ [mm]).

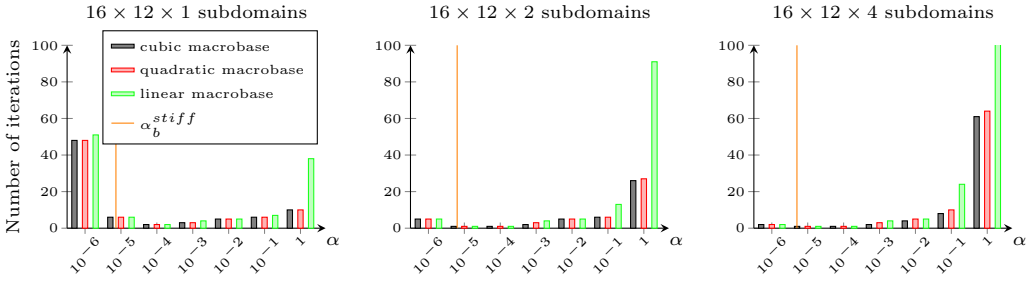

Figure 7: Iterations to convergence vs. search direction factor for different number of subdomains. h = 2 [mm]. Bending load. $(k^{-m}_{S_0S_0'})_n/(k^{-m}_{S_0S_0'})_t = 1$.

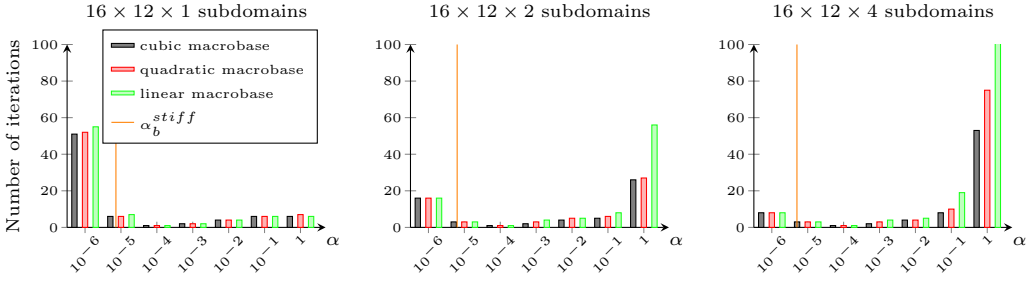

Figure 8: Iterations to convergence vs. search direction factor for different number of subdomains. h = 2 [mm]. Bending load. $(k^{-m}_{S_0S_0'})_n/(k^{-m}_{S_0S_0'})_t = (L_0/h_0)^2$.

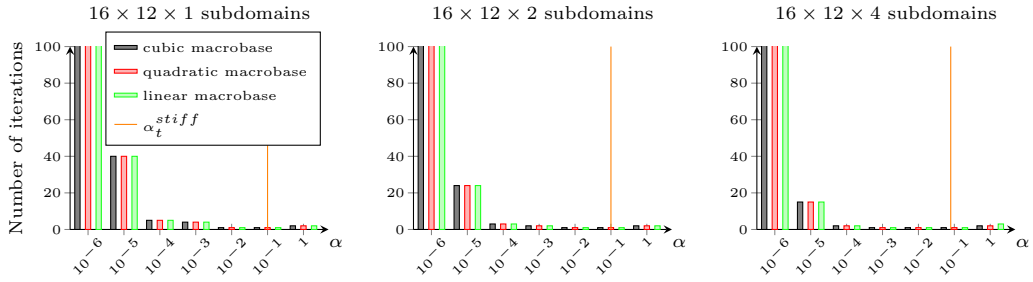

Figure 9: Iterations to convergence vs. search direction factor for different number of subdomains. h = 2 [mm]. Traction load. $(k^{-m}_{S_0S'_0})_n/(k^{-m}_{S_0S'_0})_t = 1$.

- Considering the anisotropic relation of the search direction in the bending problem, it is possible to reduce the number of iterations, but this influence is not significative when adopting the optimal search direction. In the case of a traction load, the anisotropic relation has not impact on the convergence rate.

- In bending, the classical search direction (i.e. $\alpha = 1$) is not enough to ensure the scalability of the strategy not even using the anisotropic relation. However, considering the global stiffness as the search direction, it is possible to reach a convergence rate similar to the optimal case (the maximum difference was about 6 iterations) and to conserve the same number of iterations if the number of subdomains is increased.

In order to define a more efficient and more robust strategy, we have shown that it is not necessary to enrich the macroscopic basis - the linear one is enough - if the optimal search direction is adopted, except for the case of not so slender structures in bending ($h = 8$ [mm]) for which at least quadratic terms must be considered. Then, we propose, for bending and traction problems, a new search direction which has a direct relation with the global rigidity of the structure, enabling a physical interpretation for its prediction. This value coincides with the optimal search direction in traction problems, but also gives a good approach to the optimal search direction in bending.

This result shows that the search direction $k^{-m}_{S_0S'_0}$ has a large wavelength influence and can not be interpreted in a local sense as the classical value $E/L_{\Gamma_{S_0S'_0}}$. On the other hand, using the global stiffness of the structure it is possible to achieve a faster transmission of the information. In order to estimate this rigidity, theoretical approaches or numerical solutions with a coarse mesh can be considered. The extension of this conclusion to nonlinear problems is promising, because preliminary linear calculations, in order to predict the global rigidity, can turn the strategy more efficient, as shown in the next section.

4 Nonlinear calculations

4.1 Buckling

The simulation of a 3D plate lying in the X_1X_2-plane with simply supported edges under a compressive displacement is carried out in this section. In order to induce the buckling of the plate, a transverse load, $q = 0.01$ [N/mm^2], uniformly distributed over the upper surface is considered. The plate has the following dimensions: $L_{X_1} = 160$ [mm], $L_{X_2} = 120$ [mm] and $h = 2$ [mm], and is made out of a 0° layer of the same material adopted in Sec. 3. The structure is split into 16 and 12 subdomains in the X_1 and X_2 directions, respectively, while two partitions through-the-thickness are investigated: 1 or 4 subdomains. The partition of $16 \times 12 \times 1$ subdomains has about 500 thousand DOFs in total and the second one ($16 \times 12 \times 4$ subdomains) has four time more DOFs (the number of DOFs per subdomain being fixed). Fig. 10 shows the compressive load vs. the maximal transverse displacement of the simulated plate.

This example is about combined bending and compression loads in a large displacement context. We wish to estimate the search direction factor for which the computing time is the lowest possible, using a linear macroscopic basis and the anisotropic relation of the search directions. From the conclusions of the precedent section, we propose to predict an optimal search direction factor from the global rigidity of the structure for each load case. Then, performing a preliminary linear calculation, the search direction factor associated to the bending load is $\alpha^{stiff}_{bend} = 3 \cdot 10^{-4}$ and to the traction load is $\alpha^{stiff}_{trac} = 1.2 \cdot 10^{-1}$. Finally, a mean value $\alpha^{stiff}_{bend-trac} = 6 \cdot 10^{-2}$ is proposed to the nonlinear calculation.

The results of the buckling simulations performed in 8 increments are shown in Fig. 11 and Fig. 12 for the partitions of 192 subdomains and 768 subdomains, respectively. Each figure shows the number of iterations for each increment and also the total calculation time for three search directions: the search direction α^{stiff} proposed from the rigidity of the structure, the optimal search direction α^{opt} empirically found after a set of

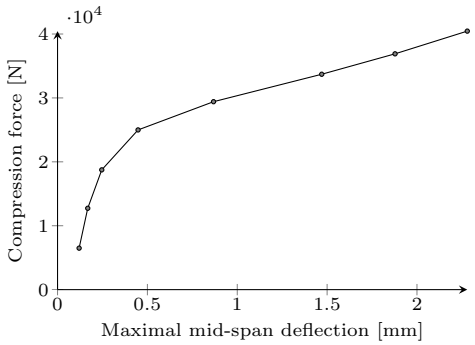

Figure 10: Load-displacement curve of a compressed plate in buckling.

calculations for $\alpha \in [10^{-5}, 10]$, and the classical search direction $\alpha^{class} = 1$. In the case of $16 \times 12 \times 1$ (respectively $16 \times 12 \times 4$) subdomains, the total number of iterations for the proposed α^{stiff} is 25% (respectively 85%) less than using the α^{class}. This enhancement to the convergence rate is encouraging since when using the optimal search direction factor α^{opt} which is not computable in practice, the gain with respect to α^{class} is 52% and 90% (for 192 and 768 subdomains, respectively).

It is important to note that when using α^{stiff} or α^{opt}, the scalability is moderately ensured because when quadrupling the number of subdomains, the number of iterations is doubled. This result is remarkably better than using α^{class} for which the number of iterations is 32 times more when quadrupling. A last observation concerns the total computing time, the partition of $16 \times 12 \times 4$ has 4 times more DOFs and the solving lasts only 6 times longer than for the partition of $16 \times 12 \times 1$ subdomains (when employing α^{stiff} or α^{opt}).

4.2 Combined buckling and delamination

In this section, the simulation of the delamination of an open hole IM7/8552 laminate loaded in compression in a nonlinear context is analyzed. The fiber orientation of the quasi-isotropic composite is $[0°/45°/90°/-45°]_S$ and the material properties are detailed in Sec. 3. The plate is 160 [mm] long (along the X_1 axis) by 120 [mm] wide (along the X_2 axis) while the total specimen thickness is 4 [mm] and the hole radius is 15 [mm]. The plate is simply supported and subjected to a compressive displacement along direction X_1 and to a transverse load, q = 0.01 [N/mm^2], uniformly distributed over the upper surface. The structure is split into 864 subdomains and the whole discretization has 2.5 million linear wedge elements with a total of 5 million DOFs (the subdomains and the material assignation is shown in Fig. 13). In order to include delamination, cohesive interfaces are taken into account between plies except for the double $-45°$ layer located in the middle of the laminate. In order to carry out the simulation efficiently, the search direction factor has been calculated from the global stiffness of the structure using the same methodology as in the precedent buckling problem (Sec. 4.1).

Fig. 13 presents the compressive load as a function of the maximum axial displacement. Delamination around the hole begins to propagate early after the first increment, but without exhibiting a softening response because the interlaminar strength does not play a significantly role in the initial behavior governed by compression.

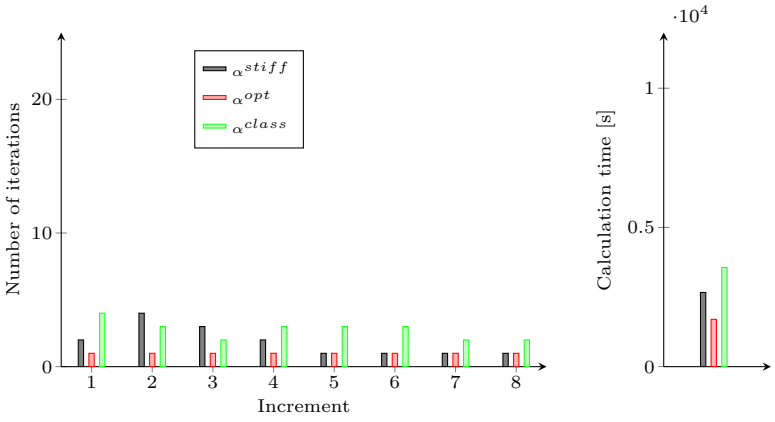

Figure 11: Iterations to convergence for each time increment of a buckling test. $16 \times 12 \times 1$ subdomains, h=2 [mm].

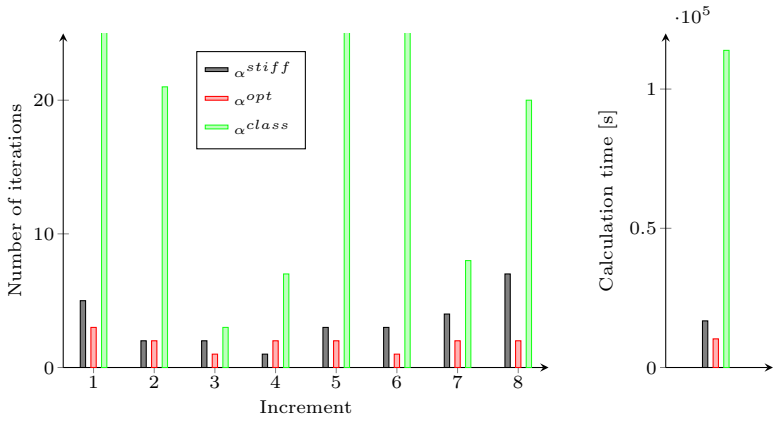

Figure 12: Iterations to convergence for each time increment of a buckling test. $16 \times 12 \times 4$ subdomains, h=2 [mm].

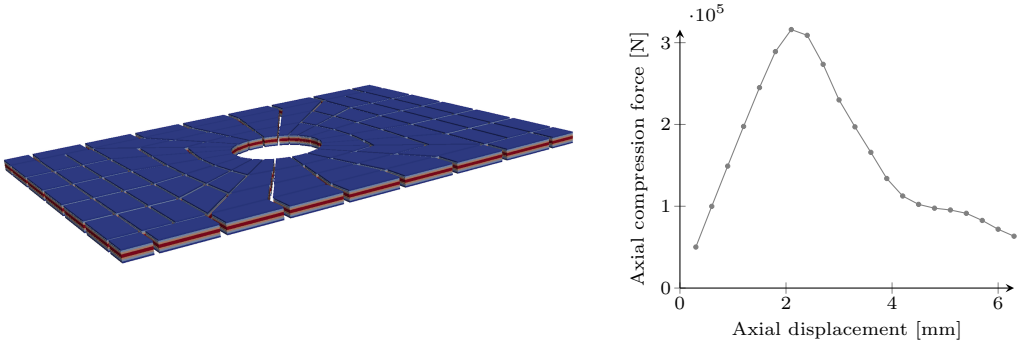

Figure 13: An open hole compression test. Partition and material assignation (left). Load-displacement response (right).

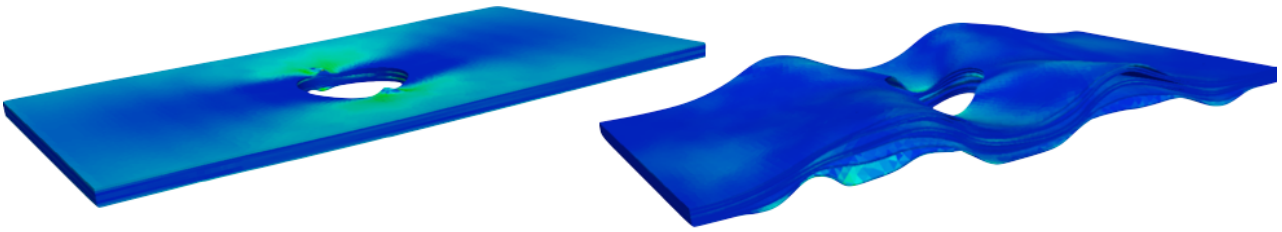

Figure 14: Stress distribution and deformation of the open hole compression test. 6^{th} increment (left) and 21^{st} increment (right).

Delamination around the hole enables the local buckling to appear at the 6^{th} step, as observed in Fig. 14 (left). Then, the plate buckles in a single wave when reaching the critical load at $3.1 \cdot 10^5$ [N] (the delamination front at this point is shown in Fig. 15). After that, delamination continues to propagate decreasing the strength of the buckled plate and gradually inducing a two-wave configuration, as shown in Fig. 14 (right). The delaminated area at the last computed increment (21^{st} step) is above 80%.

Using the proposed search direction factor α^{stiff}, the number of iterations is 73% less than when using the classical choice α^{class} at the first time step. For the following time steps, the comparison has been skipped because the calculation time for α^{class} is prohibitive (above one week per time step). Despite the effectiveness of α^{stiff}, the mean number of iterations per time step remains about 190. The augmentation compared to the buckling example (Sec. 4.1) is due to the delamination.

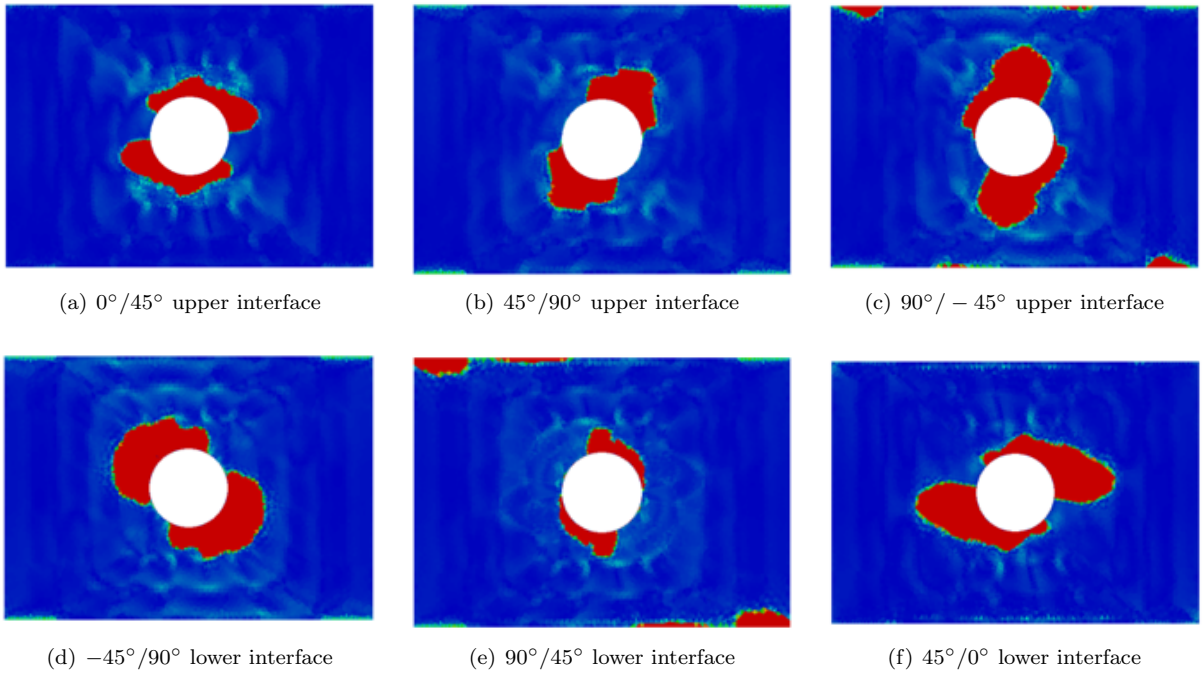

(a) $0°/45°$ upper interface (b) $45°/90°$ upper interface (c) $90°/-45°$ upper interface

(d) $-45°/90°$ lower interface (e) $90°/45°$ lower interface (f) $45°/0°$ lower interface

Figure 15: Delamination front for each interface. The damage variable d goes from 0 (blue) to 1 (red).

5 Conclusion

In this paper, the convergence rate and the scalability of a micro-macro LaTIn-based Domain Decomposition Method have been investigated. Two parameters of the method, the macroscopic space and the search directions, have been analyzed for traction, bending and buckling problems.

We observed that the number of iterations depends on the load case, the geometry and the partitioning when the classical choice of these parameters is implemented. We demonstrate that there is an optimal search direction factor for which the linear macroscopic basis is enough to minimize the number of iterations and to ensure the scalability (except for the case of not so slender structures in bending for which at least quadratic terms must be considered in the macroscopic basis).

In order to predict this optimal search direction, an approximated value calculated from the global stiffness of the structure has been proposed, enabling to compute linear and nonlinear problems efficiently. Finally, the enhanced search direction has been used to carry out the simulation of a open hole laminate subjected to a compressive load, including delamination between plies in a large displacement framework.

This paper shows us that finding an optimal search direction and/or an appropriate macroscopic space become relevant in order to achieve scalability and to optimize the convergence rate. Here, a simple approximation of the search direction without enriching the linear macroscopic basis has been proposed, but the key is to define an automatic procedure in order to capture them in a systematic way. In subsequent developments, two possibilities are considered. i) To automatically define a proper macroscopic space, as proposed in [17, 18] for FETI and BDDC. In this case, if the size of the macroscopic problem may become huge, but thanks to its sparsity its solution can be parallelized using a BDD method as was implemented in [10]. ii) To automatically find a good approximation of the optimal search direction, thus an approached Schur complement with inspiration from [21].

Acknowledgments

K. Saavedra acknowledges the financial support from CONICYT, FONDECYT Initiation into research project No 11130623.

A Definition of the macroscopic basis

We present the construction of a basis $\mathcal{B}^M_{S_0S_0'} = \left(\underline{e}^M_1, \ldots, \underline{e}^M_{N_M}\right)$ for the subspace of interface (high order) macroscopic displacements $\mathcal{W}^M_{S_0S_0'}$ for a plane interface $\Gamma_{S_0S_0'}$. Because the search direction parameter is a scalar, the

classical L^2 scalar product can be used to orthonormalize the basis.

Let $\Gamma_{S_0S_0'}$ be a plane interface, $\underline{G}$ its center of gravity, $\underline{M}$ a current point of the interface, $\mathbf{I}_{S_0S_0'} = \int_{\Gamma_{S_0S_0'}} \underline{GM} \otimes \underline{GM}\, d\Gamma_0$ the second inertia matrix and $(\underline{N}_i)_{i\in\{1,2,3\}}$ the eigenvectors of $\mathbf{I}_{S_0S_0'}$ (or the principal axes of inertia) such that the associated principal moments of inertia verify $I_1 \geq I_2 \geq I_3$. In this case, I_3 is null because the normal vector of $\Gamma_{S_0S_0'}$ and N_3 are collinear.

The usual linear macroscopic basis extract translations and rotations along the three principal axes, stretching along $\underline{N}_1$ and $\underline{N}_2$ and one in-plane shear, using the following functions, respectively (see Fig. 3):

$$\begin{array}{l} \underline{e}_1^M = \underline{N}_1 \quad ; \quad \underline{e}_2^M = \underline{N}_2 \quad ; \quad \underline{e}_3^M = \underline{N}_3 \\ \underline{e}_4^M = (\underline{N}_1 \wedge \underline{GM}) \quad ; \quad \underline{e}_5^M = (\underline{N}_2 \wedge \underline{GM}) \quad ; \quad \underline{e}_6^M = (\underline{N}_3 \wedge \underline{GM}) \\ \underline{e}_7^M = (\underline{N}_1 \cdot \underline{GM})\underline{N}_1 \quad ; \quad \underline{e}_8^M = (\underline{N}_2 \cdot \underline{GM})\underline{N}_2 \\ \underline{e}_9^M = \frac{1}{2}((\underline{N}_2.\underline{GM})\,\underline{N}_1 + (\underline{N}_1.\underline{GM})\,\underline{N}_2) \end{array}$$

In order to add quadratic terms to the macroscopic basis, we propose the following quadratic extensions and deflections along $\underline{N}_1$ and $\underline{N}_2$, and two in-plane quadratic distributions, respectively (see Fig. 3):

$$\begin{array}{l} \underline{e}_{10}^M = (\underline{N}_1 \cdot \underline{GM})^2\underline{N}_1 \quad ; \quad \underline{e}_{11}^M = (\underline{N}_2 \cdot \underline{GM})^2\underline{N}_2 \\ \underline{e}_{12}^M = (\underline{N}_1 \cdot \underline{GM})^2\underline{N}_3 \quad ; \quad \underline{e}_{13}^M = (\underline{N}_2 \cdot \underline{GM})^2\underline{N}_3 \\ \underline{e}_{14}^M = \frac{1}{2}((\underline{N}_1.\underline{GM})^2\,\underline{N}_2 - (\underline{N}_2.\underline{GM})^2\,\underline{N}_1) \\ \underline{e}_{15}^M = \frac{1}{2}((\underline{N}_2.\underline{GM})^2\,\underline{N}_1 + (\underline{N}_1.\underline{GM})^2\,\underline{N}_2) \end{array}$$

Finally, we consider cubic extensions and deflections along $\underline{N}_1$ and $\underline{N}_2$, a cubic rotation along $\underline{N}_3$ and one in-plane shear distribution, as respectively detailed in the following functions:

$$\begin{array}{l} \underline{e}_{16}^M = (\underline{N}_1 \cdot \underline{GM})^3\underline{N}_1 \quad ; \quad \underline{e}_{17}^M = (\underline{N}_2 \cdot \underline{GM})^3\underline{N}_2 \\ \underline{e}_{18}^M = (\underline{N}_1 \cdot \underline{GM})^3\underline{N}_3 \quad ; \quad \underline{e}_{19}^M = (\underline{N}_2 \cdot \underline{GM})^3\underline{N}_3 \\ \underline{e}_{20}^M = \frac{1}{2}((\underline{N}_1.\underline{GM})^3\,\underline{N}_2 - (\underline{N}_2.\underline{GM})^3\,\underline{N}_1) \\ \underline{e}_{21}^M = \frac{1}{2}((\underline{N}_2.\underline{GM})^3\,\underline{N}_1 + (\underline{N}_1.\underline{GM})^3\,\underline{N}_2) \end{array}$$

In order to orthonormalize the set of macroscopic functions, the Gram-Schmidt method is used.

References

[1] C. Farhat, F.-X. Roux, A method of finite element tearing and interconnecting and its parallel solution algorithm, Int. J. Numer. Meth. Engng. 32 (1991) 1205–1227.

[2] J. Mandel, Balancing domain decomposition, Communications in Numerical Methods in Engineering 9 (1993) 233–241.

[3] C. Farhat, M. Lesoinne, P. LeTallec, K. Pierson, D. Rixen, FETI-DP: A Dual-Primal unified FETI method - part I: A faster alternative to the two-level FETI method, International Journal for Numerical Methods in Engineering 7 (2001) 1523–1544.

[4] C. R. Dohrmann, A preconditionner for substructuring based on constrained energy minimization, SIAM Journal for Scientific Computing 25 (2003) 246.

[5] P. Gosselet, C. Rey, Non-overlapping domain decomposition methods in structural mechanics, Archives of Computational Methods in Engineering 13 (2006) 515–572.

[6] P. Ladevèze, O. Loiseau, D. Dureisseix, A micro-macro and parallel computational strategy for highly heterogeneous structures, International Journal for Numerical Methods in Engineering 52 (1-2) (2001) 121–138.

[7] V. Roulet, L. Champaney, P.-A. Boucard, A parallel strategy for the multiparametric analysis of structures with large contact and friction surfaces, Advances in Engineering Software 42 (6) (2011) 347 – 358.

[8] P. A. Guidault, O. Allix, L. Champaney, C. Cornuault, A multiscale extended finite element method for crack propagation, Computer Methods in Applied Mechanics and Engineering 197 (5) (2008) 381–399.

[9] E. I. Saavedra Flores, K. Saavedra, J. Hinojosa, Y. Chandra, R. Das, Multi-scale modelling of rolling shear failure in cross-laminated timber structures by homogenisation and cohesive zone models, International Journal of Solids and Structures 81 (2016) 219 – 232.

[10] P. Kerfriden, O. Allix, P. Gosselet, A three-scale domain decomposition method for the 3D analysis of debonding in laminates, Computational Mechanics 44 (3) (2009) 343–362.

[11] K. Saavedra, O. Allix, P. Gosselet, On a multiscale strategy and its optimization for the simulation of combined delamination and buckling, International Journal for Numerical Methods in Engineering 91 (7) (2012) 772–798.

[12] C. Farhat, N. Maman, G. W. Brown, Mesh partitioning for implicit computations via iterative domain decomposition: Impact and optimization of the subdomain aspect ratio, International Journal for Numerical Methods in Engineering 38 (6) (1995) 989–981000.

[13] A. Klawonn, O. Rheinbach, O. B. Widlund, An analysis of a FETI–DP algorithm on irregular subdomains in the plane, SIAM Journal on Numerical Analysis 46 (5) (2008) 2484–2504.

[14] J. Mandel, M. Brezina, Balancing domain decomposition for problems with large jumps in coefficients, Mathematics of Computation 65 (216) (1996) 1387–1402.

[15] C. Pechstein, R. Scheichl, Analysis of FETI methods for multiscale PDEs, Numerische Mathematik 111 (2) (2008) 293–333.

[16] C. Pechstein, R. Scheichl, Analysis of FETI methods for multiscale PDEs. part II: interface variation, Numerische Mathematik 118 (3) (2011) 485–529.

[17] N. Spillane, D. Rixen, Automatic spectral coarse spaces for robust finite element tearing and interconnecting and balanced domain decomposition algorithms, International Journal for Numerical Methods in Engineering 95 (11) (2013) 953–990.

[18] L. B. da Veiga, L. F. Pavarino, S. Scacchi, O. B. Widlund, S. Zampini, Isogeometric BDDC preconditioners with deluxe scaling, SIAM Journal on Scientific Computing 36 (3) (2014) A1118–A1139.

[19] P. Gosselet, D. Rixen, F. Roux, N. Spillane, Simultaneous FETI and block FETI: robust domain decomposition with multiple search directions, International Journal for Numerical Methods in Engineering.

[20] A. Klawonn, M. Kühn, O. Rheinbach, Adaptive coarse spaces for FETI-DP in three dimensions, SIAM Journal on Scientific Computing 38 (5) (2016) A2880–A2911.

[21] L. Gendre, O. Allix, P. Gosselet, A two-scale approximation of the schur complement and its use for non-intrusive coupling, International Journal for Numerical Methods in Engineering 87 (9) (2011) 889–905.

[22] J. Pebrel, C. Rey, P. Gosselet, A nonlinear dual domain decomposition method: application to structural problems with damage, International Journal for Multiscale Computational Engineering 6 (3) (2008) 251–262.

[23] A. Klawonn, M. Lanser, O. Rheinbach, Nonlinear feti-dp and bddc methods, SIAM Journal on Scientific Computing 36 (2) (2014) A737–A765.

[24] J. Hinojosa, O. Allix, P.-A. Guidault, P. Cresta, Domain decomposition methods with nonlinear localization for the buckling and post-buckling analyses of large structures, Advances in Engineering Software 70 (2014) 13 – 24.

[25] C. Negrello, P. Gosselet, C. Rey, J. Pebrel, Substructured formulations of nonlinear structure problems – influence of the interface condition, International Journal for Numerical Methods in Engineering 107 (13) (2016) 1083–1105.

[26] O. Dubois, M. J. Gander, Domain Decomposition Methods in Science and Engineering XVIII, Springer, Berlin, Heidelberg, 2009, Ch. Convergence Behavior of a Two-Level Optimized Schwarz Preconditioner, pp. 177–184.

[27] R. Glowinski, Variational Methods for the Numerical Solution of Nonlinear Elliptic Problems, Society for Industrial and Applied Mathematics, Philadelphia, PA, 2015.

[28] O. Allix, A. Corigliano, Geometrical and interfacial non-linearities in the analysis of delamination in composites, International Journal of Solids and Structures 36 (15) (1999) 2189–2216.

[29] P. Ladevèze, Nonlinear Computational Structural Mechanics - New Approaches and Non-incremental Methods of Calculation, Springer-Verlag, Berlin, 1999.

[30] P. Ladevèze, A. Nouy, On a multiscale computational strategy with time and space homogenization for structural mechanics, Computer Methods in Applied Mechanics and Engineering 192 (28-30) (2003) 3061–3087.

[31] R. Haferssas, P. Jolivet, F. Nataf, A robust coarse space for optimized Schwarz methods SORAS-GenEO-2, C. R. Math. Acad. Sci. Paris 353 (2015) 959–963.

[32] P. Kerfriden, Stratégie de décomposition de domaine à trois échelles pour la simulation du délaminage dans les stratifiés, Ph.D. thesis, ENS de Cachan (2008).

[33] O. Allix, P. Gosselet, P. Kerfriden, K. Saavedra, Virtual delamination testing through non-linear multi-scale computational methods: some recent progress, Computers, Materials & Continua 32 (2) (2012) 107–132.

[34] O. Allix, D. Lévêque, L. Perret, Identification and forecast of delamination in composite laminates by an interlaminar interface model, Composites Science and Technology 58 (5) (1998) 671–678.

[35] A. Corigliano, O. Allix, Some aspects of interlaminar degradation in composites, Computer Methods in Applied Mechanics and Engineering 185 (2-4) (2000) 203–224.

[36] O. Allix, P. Kerfriden, P. Gosselet, On the control of the load increments for a proper description of multiple delamination in a domain decomposition framework, International Journal for Numerical Methods in Engineering 83 (11) (2010) 1518–1540.

[37] L. Champaney, J. Y. Cognard, P. Ladèveze, Modular analysis of assemblages of three-dimensional structures with unilateral contact conditions, Computers & Structures 73 (1-5) (1999) 249 – 266.

[38] F. Daghia, P. Ladeveze, Identification and validation of an enhanced mesomodel for laminated composites within the WWFE-III, Journal of Composite Materials 47 (20-21) (2013) 2675–2693.